NPS ARCHIVE
1958
RICCI, W.

TRANSFER FUNCTION OF A URANIUM-GRAPHITE SUBCRITICAL ASSEMBLY

WILLIAM JOHN RICCI

LIBRARY

TRANSFER FUNCTION OF A URANIUM-GRAPHITE SUBCRITICAL ASSEMBLY

by

William John Ricci

A Thesis Submitted to the
Graduate Faculty in Partial Fulfillment of
The Requirements for the Degree of
MASTER OF SCIENCE

Major Subject: Nuclear Engineering

TABLE OF CONTENTS

	Page
INTRODUCTION	1
REVIEW OF THE LITERATURE	3
DERIVATION OF THE TRANSFER FUNCTION	5
DESCRIPTION OF APPARATUS AND EXPERIMENTAL PROCEDURE	13
DISCUSSION OF RESULTS	30
CONCLUSIONS	39
SUGGESTIONS FOR FURTHER STUDY	41
LITERATURE CITED	42
ACKNOWLEDGMENTS	44
APPENDIX	45

37505

INTRODUCTION

The role of the subcritical assembly is gradually being enlarged to include studies of transient or dynamic responses. Demands for an inexpensive and quick method for determining the effect of various parameters upon control response have led investigations into the utilization of the assembly for such purposes. Perhaps the most important advantage of the subcritical assembly is the ease with which experiments may be performed. Extra physical safeguards and restrictions are at a minimum, and no extensive shielding is required. The relatively small size of the subcritical assembly also tends to make it easier and less expensive to vary the desired parameters.

Borrowing from servomechanism theory and treating the assembly as a "black box", many investigators have aptly applied the concept of the transfer function to describe the response to a given forcing function. In practice, phase and amplitude relations, when considered as functions of the driving frequency, are collectively designated as the assembly transfer function.

The parametric forcing or driving function is of two types, reactivity forcing and source forcing. In general,

reactivity forcing is represented by the change in neutron density due to a small harmonic variation in the reactivity, that is, a harmonic change in the reactor geometry accomplished by oscillating some neutron absorber. Source forcing, in contrast to reactivity forcing, in no way affects or changes the assembly geometry. It is merely an imposed variation in the primary source.

The objective of this thesis is to present the subcritical assembly transfer function which was determined by the technique of source forcing.

REVIEW OF THE LITERATURE

The history of the subcritical pile and its role in the development of the first self-sustaining chain reaction has become legend (1), but work is continuing (2) to make the assembly a testing vehicle and not merely an object of investigation for itself.

The initial servomechanism concept was presented by Pigott, Crever, and Owens (9 and 10) at the Knolls Atomic Power Laboratory. Because the roots of the kinetics equation are negative, the pile transfer function was noted as being the same as that for a minimum phase shift network. This permitted it to be represented by a Bode diagram. A pile kinetic simulator, whose voltage response represented the pile neutron flux response, was successfully utilized for the test to determine the stability of an automatic control system and its ability to maintain a desired power level.

Franz (5) determined substantially the same type transfer function but used a more sophisticated approach. By definition, the transfer function relates sinusoidal variations; hence it can be handled by the standard techniques of servomechanism theory. The ratio of the Laplace transform of the output to that of the input was found to give the transfer function more conveniently. In both the above situations it

was carefully noted that the functions determined were those of a pile simulator and described the pile responses only to the same degree that the equations utilized described the conditions in the pile.

It remained for Harrer, Boyar, and Krucoff (8), based on their now classical experiment on the Argonne CP-2 reactor, to justify the use of the transfer function to describe a reactor as a control loop element. Since their experiment it has become standard procedure to determine the transfer function of critical assemblies and reactors for stability criteria. This method has also been applied to mockups of proposed reactors. Boland, Smith, and Rice (3) found the zero power transfer function of the ZPR-III mockup assembly of the ZPR-I, a fast critical assembly. The results were used to determine the best oscillator rods and measurement techniques to be used on the actual assembly, when constructed.

In all the references found, the information primarily pertained to a critical assembly and to the solution of the transfer function by reactivity forcing. Other than a cursory discussion in Glasstone (6, p. 252), no unclassified reference was found which contained any information concerning the transfer function of a subcritical assembly as such or concerning source forcing.

DERIVATION OF THE TRANSFER FUNCTION

The response of the subcritical assembly to source forcing can be derived from the time-dependent general diffusion equation. For simplicity all neutrons are considered thermal, and hence the equation can be written as (7, p. 101)

$$D \nabla^2 \phi - \Sigma_a \phi + S = \frac{\partial n}{\partial t} = \frac{1}{\nu} \frac{\partial \phi}{\partial t} \qquad \text{Eq. 1}$$

where ν is the mean velocity of the thermal neutrons. In general the symbols in the derivation are in common usage (6, pp. 223-253), but the meanings are given in the List of Symbols for convenient reference.

The source term is made up of three parts. The first portion is the prompt neutrons resulting from fission. According to the Fermi age theory this prompt neutron source term may be expressed as

$$S_p = (1 - \beta) k_\infty \Sigma_a \phi e^{-B^2 \tau} \qquad \text{Eq. 2}$$

where β is the total fraction of delayed neutrons in any one generation. The second portion is the delayed neutrons which result from fission and which are given off during the decay of certain fission products. Generally, six groups are recognized, each group having a discrete decay constant λ_i

List of Symbols

B^2	Buckling	$cm.^{-2}$
β	Fraction of average group of delayed neutrons	
β_i	Fraction of i^{th} group of delayed neutrons	
C	Concentration of average group of delayed neutron precursors	
C_i	Concentration of i^{th} group of delayed neutron precursors	
D	Thermal neutron diffusion coefficient	cm.
k	Effective multiplication factor	
k_∞	Multiplication factor for an infinite assembly	
L	Neutron diffusion length in the moderator	cm.
ℓ	Average neutron lifetime in a finite assembly	sec.
ℓ_o	Mean neutron lifetime in an infinite assembly	sec.
λ	Decay constant of average group of delayed neutron precursors	$sec.^{-1}$
λ_i	Decay constant of the i^{th} group of delayed neutron precursors	$sec.^{-1}$
n	Number of neutrons of thermal energies	
p	Resonance escape probability	
ϕ	Thermal neutron flux	$\frac{\text{neutrons}}{cm.^2\ sec.}$
S	Rate of production of source neutrons	$\frac{\text{neutrons}}{sec.}$
Σ_a	Macroscopic absorption crossection	$cm.^{-1}$
t	Time	sec.
τ	Fermi age	$cm.^2$
ν	Thermal neutron mean velocity	cm./sec.
ω	Frequency of oscillation	$\frac{\text{radians}}{sec.}$

and fraction β_i (11, p. 14). With C_i defined as the concentration of the i^{th} group of delayed neutron emitters, the net rate of formation of the precursor is given by

$$\frac{\partial C_i}{\partial t} = \beta_i \frac{k_\infty}{p} \Sigma_a \phi - \lambda_i C_i. \qquad \text{Eq. 3}$$

Since the rate of production of the delayed neutrons is numerically equal to the decay rate of the precursor, this rate equals $\sum_{i=1}^{6} \lambda_i C_i$ for the six groups under consideration. With the Fermi age of a delayed neutron assumed equal to that of a prompt neutron, the slowing-down nonleakage probability will be $e^{-B^2\tau}$. This is not strictly true because the energy of the delayed neutrons is generally less than the average energy of the prompt neutrons, but the approximation is considered reasonable (6, p. 227). The delayed neutron source term may be written as

$$S_d = p\, e^{-B^2\tau} \sum_{i=1}^{6} \lambda_i C_i \qquad \text{Eq. 4}$$

where p is defined as the resonance escape probability. The third portion is the external source term which will be defined as

$$S_e = S_o + S_1 e^{j\omega t} \qquad \text{Eq. 5}$$

where S_1 is the complex amplitude.

For further simplification of the mathematics, the space and time variables will be considered separable so that the partial differential equations may be reduced to ordinary

differential equations (6, p. 227).

With substitution of Equations 2, 4, and 5 into Equation 1, the resulting expression is

$$D\nabla^2\phi - \Sigma_a\phi + (1-\beta)k_\infty\Sigma_a\phi e^{-B^2\tau} + p\,e^{-B^2\tau}\sum_{i=1}^{6}\lambda_i C_i + (S_o+S_1 e^{j\omega t}) = \frac{1}{v}\frac{d\phi}{dt}. \qquad \text{Eq. 6}$$

Only first modes will be considered for the simplified solution, and hence $\nabla^2\phi = -B^2\phi$ (8, p. 33). By definition ℓ_o is the mean lifetime of the thermal neutrons in an infinite medium, and it equals $\frac{1}{\Sigma_a v}$. With division by Σ_a and the above substitutions, Equation 6 becomes

$$-(L^2B^2+1)\phi + (1-\beta)k_\infty e^{-B^2\tau}\phi + \frac{p}{\Sigma_a}e^{-B^2\tau}\sum_{i=1}^{6}\lambda_i C_i + \frac{S_o+S_1 e^{j\omega t}}{\Sigma_a} = \ell_o\frac{d\phi}{dt}. \qquad \text{Eq. 7}$$

Let

$$k = \frac{k_\infty e^{-B^2\tau}}{1 + L^2B^2} \qquad \text{Eq. 8}$$

and

$$\ell = \frac{\ell_o}{1 + L^2B^2}, \qquad \text{Eq. 9}$$

where k is the effective multiplication factor and ℓ is the average thermal neutron lifetime, both in a finite assembly. With term rearrangement and with substitution of k and ℓ, it is possible to write Equation 7 as

$$-\phi + (1-\beta)k\phi + \frac{p}{\Sigma_a}\frac{k}{k_\infty}\sum_{i=1}^{6}\lambda_i C_i + \frac{S_o + S_1 e^{j\omega t}}{\Sigma_a(1 + L^2B^2)}$$

$$= l\frac{d\phi}{dt}. \qquad \text{Eq. 10}$$

With division by l, collection of the terms containing ϕ, and substitution of $\phi = n\nu$, where ν is considered constant, Equation 10 reduces to

$$\left(k(1-\beta) - 1\right)\frac{n\nu}{l} + \frac{p}{\Sigma_a}\frac{k}{l k_\infty}\sum_{i=1}^{6}\lambda_i C_i + \frac{S_o + S_1 e^{j\omega t}}{\Sigma_a l(1+L^2B^2)}$$

$$= \nu\frac{dn}{dt}. \qquad \text{Eq. 11}$$

From the above definitions 8 and 9

$$\frac{k}{l k_\infty} = \frac{e^{-B^2\tau}}{l_o},$$

but since

$$l_o = \frac{1}{\Sigma_a \nu}$$

$$\frac{k}{l k_\infty} = e^{-B^2\tau}\Sigma_a\nu. \qquad \text{Eq. 12}$$

In the same manner

$$l_o = l(1 + L^2B^2) = \frac{1}{\Sigma_a\nu}$$

or

$$\frac{1}{\nu} = \Sigma_a l(1 + L^2B^2). \qquad \text{Eq. 13}$$

With these substitutions and division by ν, Equation 11 becomes

$$\left(k\,(1-\beta)-1\right)\frac{n}{\ell}+p\,e^{-B^2\tau}\sum_{i=1}^{6}\lambda_i C_i+S_o+S_1 e^{j\omega t}$$

$$=\frac{dn}{dt}. \qquad \text{Eq. 14}$$

From Equations 3, 8, and 13 it follows that

$$\frac{dC_i}{dt}=\beta_i\frac{k\,n}{p\ell\,e^{-B^2\tau}}-\lambda_i C_i. \qquad \text{Eq. 15}$$

With rearrangement of Equation 15 and with substitution for $\lambda_i C_i$, Equation 14 becomes

$$\left(k(1-\beta)-1\right)\frac{n}{\ell}+p\,e^{-B^2\tau}\sum_{i=1}^{6}\left[\frac{\beta_i k\,n}{p\,e^{-B^2\tau}\ell}-\frac{dC_i}{dt}\right]$$

$$+S_o+S_1 e^{j\omega t}=\frac{dn}{dt}, \qquad \text{Eq. 16}$$

and with rearrangement

$$(k-1)\frac{n}{\ell}-p\,e^{-B^2\tau}\sum_{i=1}^{6}\frac{dC_i}{dt}+S_o+S_1 e^{j\omega t}=\frac{dn}{dt}. \qquad \text{Eq. 17}$$

The solution for n becomes

$$n=\frac{\ell}{(k-1)}\left[p\,e^{-B^2\tau}\sum_{i=1}^{6}\frac{dC_i}{dt}+\frac{dn}{dt}\right]+\frac{\ell\,(S_o+S_1 e^{j\omega t})}{(1-k)}. \qquad \text{Eq. 18}$$

With source forcing, k will be a constant because the pile geometry is not changed. The corresponding forcing value of neutron density will be

$$n=n_o+n_1 e^{j\omega t} \qquad \text{Eq. 19}$$

where n_o is the steady component and n_1 is the complex amplitude. In an analogous manner

$$C_i=C_{oi}+C_{1i}e^{j\omega t}. \qquad \text{Eq. 20}$$

$$\left(\frac{1}{2}\right)^{\frac{n}{2}} \int_0^{\infty} e^{-\frac{x}{2}} x^{\frac{n}{2}-1} dx$$

$$= \frac{n}{2}$$

By combination of Equations 15, 19, and 20, Equation 18 becomes

$$n_o + n_1 e^{j\omega t} = \frac{\ell}{(k-1)}\left[p\, e^{-B^2\tau}\sum_{i=1}^{6}\left\{\frac{\beta_i k}{\ell p\, e^{-B^2\tau}}(n_o+n_1 e^{j\omega t}) - \lambda_i(C_{oi}+C_{1i}e^{j\omega t})\right\} + \frac{d}{dt}(n_o+n_1 e^{j\omega t})\right] + \frac{\ell(S_o+S_1 e^{j\omega t})}{(1-k)}. \qquad \text{Eq. 21}$$

Only one average group of delayed neutrons will be considered in order to make the equation more wieldy. This introduces some additional, but small, error into the results (6, p. 251). Equation 21 is the complete form, but by the definition of a transfer function only the sinusoidal portion is of concern. With separation of the steady and sinusoidal components and with the group notation dropped, the sinusoidal portion of Equation 21 becomes

$$n_1 e^{j\omega t} = \frac{\ell}{(k-1)}\left[\frac{\beta k}{\ell} n_1 e^{j\omega t} - p\, e^{-B^2\tau}\lambda C_1 e^{j\omega t} + \frac{d}{dt}(n_1 e^{j\omega t})\right] + \frac{\ell S_1 e^{j\omega t}}{(1-k)}. \qquad \text{Eq. 22}$$

Substitution of Equations 19 and 20 into Equation 15 gives

$$\frac{k\beta}{p\, e^{-B^2\tau}\ell}(n_o+n_1 e^{j\omega t}) = \lambda(C_o+C_1 e^{j\omega t}) + \frac{d}{dt}(C_o+C_1 e^{j\omega t}). \qquad \text{Eq. 23}$$

The sinusoidal portion of Equation 23 becomes

$$\frac{k\beta}{p\ell e^{-B^2\tau}} n_1 e^{j\omega t} = \lambda C_1 e^{j\omega t} + j\omega C_1 e^{j\omega t}, \qquad \text{Eq. 24}$$

or

$$\frac{\beta k n_1}{(\lambda + j\omega) C_1} = p\ell e^{-B^2\tau}. \qquad \text{Eq. 25}$$

Substitution of Equation 25 into Equation 22 gives

$$n_1 e^{j\omega t} = \frac{\beta k n_1 e^{j\omega t}}{(k-1)} - \frac{\lambda C_1 e^{j\omega t}}{(k-1)} \left[\frac{\beta k n_1}{(\lambda + j\omega) C_1}\right] + \frac{\ell j\omega n_1 e^{j\omega t}}{(k-1)} + \frac{\ell S_1 e^{j\omega t}}{(1-k)}. \qquad \text{Eq. 26}$$

With the transfer function defined as the ratio of the response to the sinusoidally varying driving force, the desired ratio is

$$\frac{n_1}{\frac{\ell S_1}{1-k}}.$$

By rearrangement Equation 26 becomes

$$n_1 \left(\frac{1-k}{\ell S_1}\right) = \frac{1}{\left(1 + \frac{\beta k}{1-k} - \frac{\lambda k \beta}{(\lambda + j\omega)(1-k)} + \frac{\ell j\omega}{(1-k)}\right)}. \qquad \text{Eq. 27}$$

The denominator of the right side of Equation 27 may be simplified to give the desired final form,

$$n_1\left(\frac{1-k}{\ell S_1}\right) = \frac{1 + \frac{j\omega}{\lambda}}{1 - \frac{\omega^2 \ell}{\lambda(1-k)} + \frac{j\omega}{\lambda}\left[1 + \frac{\lambda\ell + \beta k}{(1-k)}\right]} \cdot \quad \text{Eq. 28}$$

DESCRIPTION OF APPARATUS AND EXPERIMENTAL PROCEDURE

Figure 1 is an overall view of the subcritical assembly with the east cover removed. Reactor grade graphite cylinders 60 inches long and 7 inches in diameter were machined to a square form 6 inches across, leaving rounded corners. These were stacked in ten columns nine rows high. Additional cylinders were cut to a 5-inch high by 6-inch wide form for the top five rows. The final pile size, with the machined cylinders stacked fourteen rows high and ten columns wide, measures 60 by 60 by 79 inches. The whole array of graphite is surrounded by a sandwich of plywood, 0.010 inch cadmium, and masonite, bolted in sections and braced with a framework. The east and west covers are removable to gain access to the pile.

The graphite is placed on a wooden base constructed so that there are three accessible spaces under the pile. These spaces extend the north-south width of the assembly. Two aluminum tanks, also extending the width of the pile, were filled with water and placed in the two outermost spaces to moderate the neutrons and to reduce radiations coming directly from the sources beneath the pile. The central space was used to house the oscillator shown in Figure 2.

Figure 1. The subcritical assembly

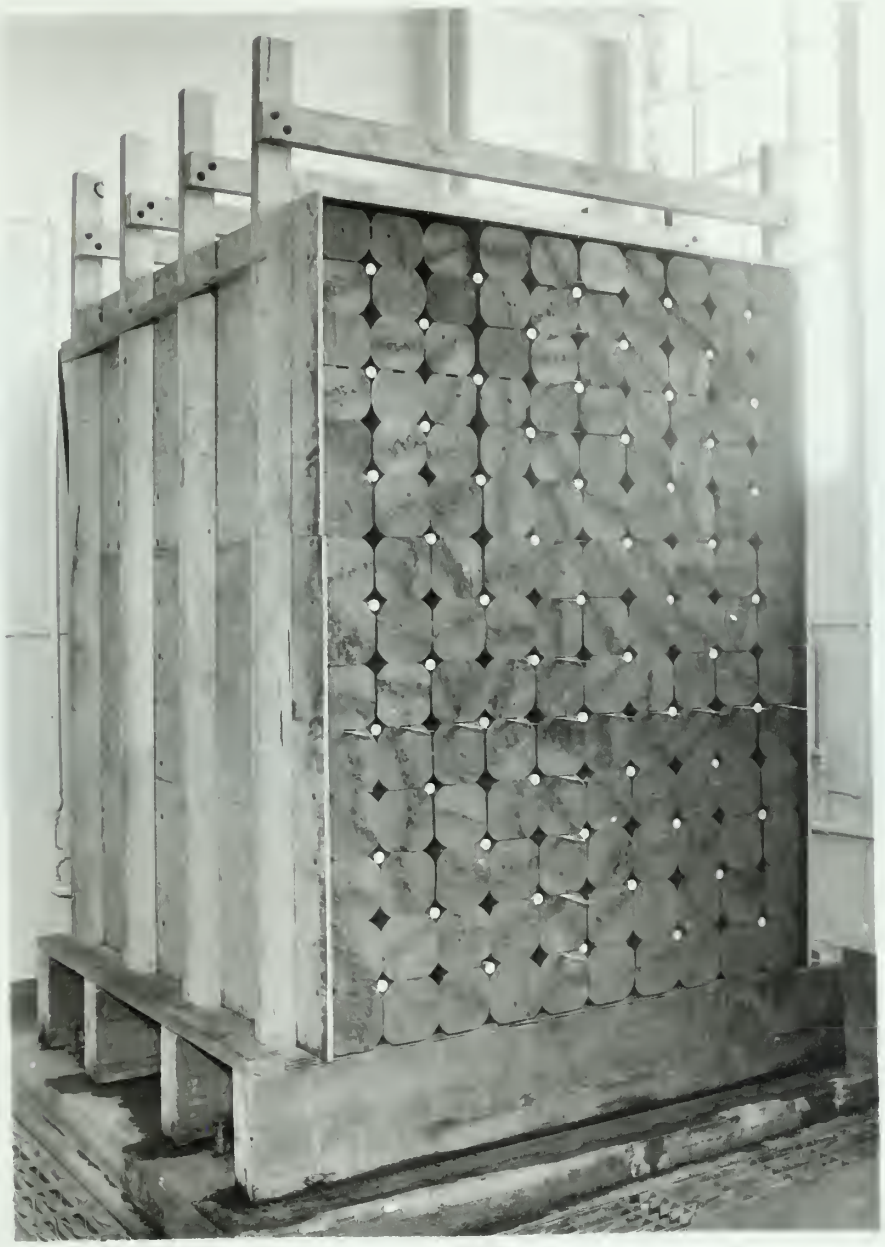

Figure 2. The oscillator assembly

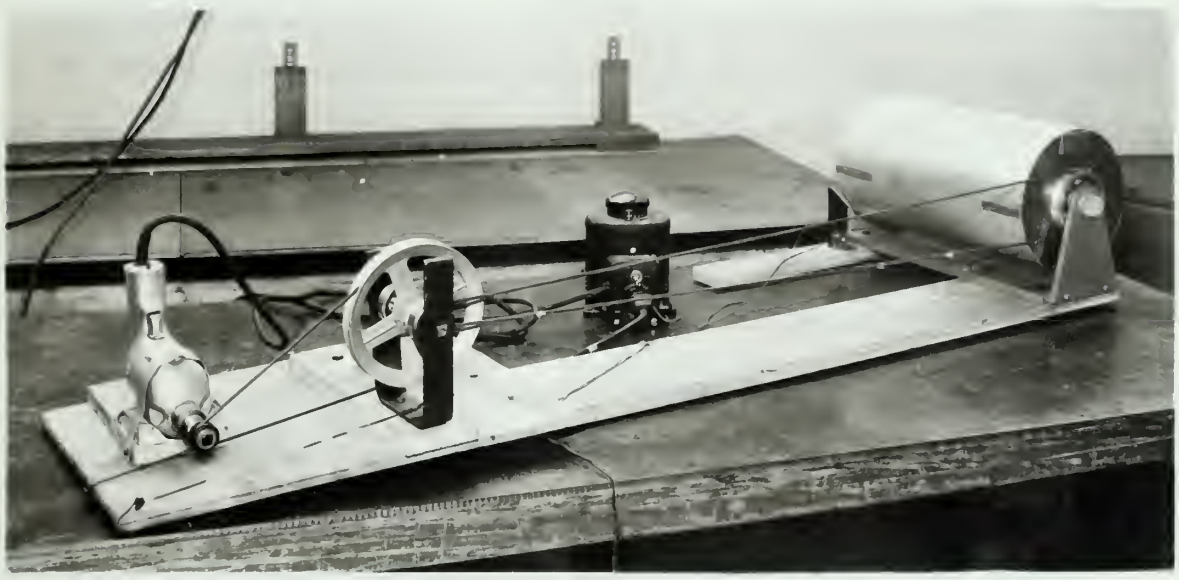

The holes between the graphite blocks, measuring approximately 1¾ inches across, permit insertion of the fuel elements in various lattice arrangements. Aluminum cylinders approximately 62 inches long each containing seven 8.2-inch uranium slugs constitute the fuel elements.

The east cover was in place during the test runs, and five holes were drilled on the cover centerline at distances of one foot, two feet, three feet, four feet, and five feet from the base. For all further discussion these holes will be designated by ordinals with the hole one foot above the base being called the first hole, the hole two feet above the base being called the second hole, and so on. With the 8.5-inch lattice, as shown in Figure 1, the cover holes were in line with empty holes between the graphite blocks, permitting a neutron detector to be inserted into the pile.

The apparatus used was assembled from readily available material and parts. Extreme accuracy and refinement of design were not attempted. Five Pu-Be sources cylindrical in shape, each measuring 1 inch in diameter and 1 3/8 inches high, were placed in the source retainer of the oscillator shown in Figures 2 and 3. Moderation was provided by a paraffin jacket formed about the source retainer. The jacket was made by rolling 1/16-inch aluminum sheet to an outside diameter of 7 3/8 inches and cementing it to 1/8-inch end plates. This container was filled by means of a filler

hole with 25 pounds of high melting point white paraffin and slowly cooled to minimize the possibility of shrinkage voids. Approximately three inches of paraffin surrounded the sources. The retainer acted as support for both the non-rotating paraffin jacket and the bearings on which the external cylinder rotated.

The rotating cylinder was formed by rolling 1/8-inch aluminum sheet to an outside diameter of 8 inches and cutting it to a length of 15 inches. The end plates, also of aluminum, were from ¼ inch stock, shrink fitted and screwed to a collar fitted on the bearing outer run casing. The cylinder was screwed onto the end plates permitting disassembly. The sine pattern was cut from a 0.010-inch thick sheet of cadmium to the dimensions shown in Figure 3 and cemented with an aluminum based cement to the inside of the rotating cylinder.

For further discussion position 1 will be used to refer to the rotating cylinder and pattern position whenever point A of the flattened pattern in Figure 3 is top dead center. Position 2 will be used to indicate that point B is top dead center. Based on the difference of readings taken with the cadmium pattern in the two extreme positions, it is estimated that approximately 20 per cent of the source neutrons reached thermal speeds in the paraffin. It is also estimated from the accepted macroscopic absorption cross section of cadmium

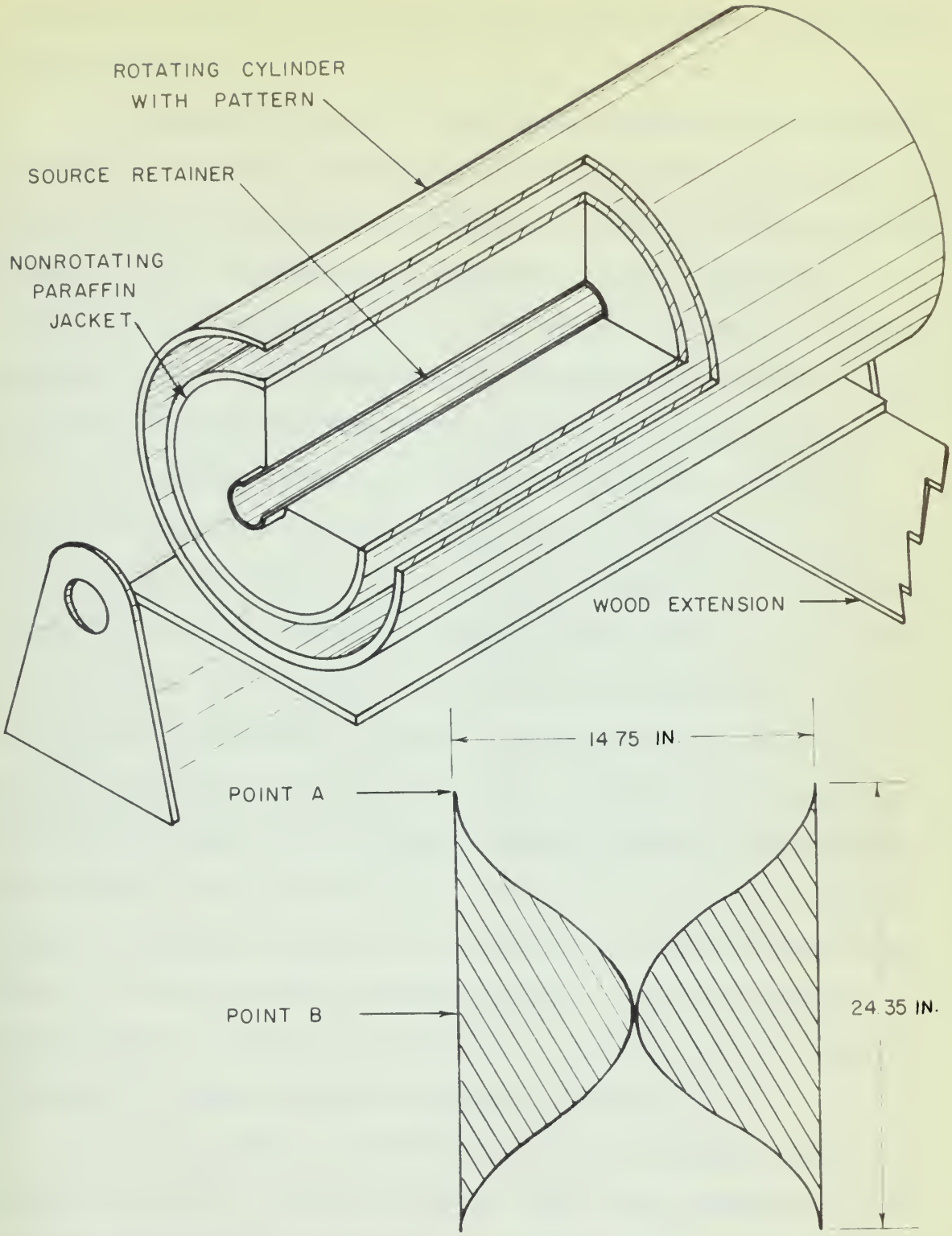

Figure 3. Oscillator and cadmium pattern detail

that 98 per cent of the thermal neutrons reaching the pattern were absorbed.

An extension of one of the bearing collars was grooved to hold the leather driving belt. The rotation frequency was varied by controlling the voltage to a ¼-inch Black and Decker electric drill mounted on a four-foot wooden extension. A speed reducer was interposed to permit speeds down to approximately 5 RPM. The oscillator was designed for speeds as high as 1000 RPM, but no tests were carried out in this range.

For maximum signal the neutron detector, a 3/8-inch diameter, 8-inch long tube filled with enriched BF_3 gas, was inserted in the first hole to the pile midpoint. A Radiation Instrument Development Laboratories, model 200-I, scaler was used for the high voltage and initial amplification. The amplifier-discriminator jumper was disconnected and the amplifier output taken directly to a Nuclear Chicago model 1615 survey meter with the high voltage rendered inoperative. The output of the survey meter was fed to a type 112 direct coupled Tektronix amplifier and thence to one amplifier and pen of a two pen Brush recording system. The instrument arrangement is pictured in Figure 4, and all the circuitry utilized is shown by block diagram in Figure 5.

The time applied variation in source strength was recorded by means of brush contacts which were mounted on the oscillator frame and the rotor and which were wired parallel

Figure 4. Electronic instrumentation

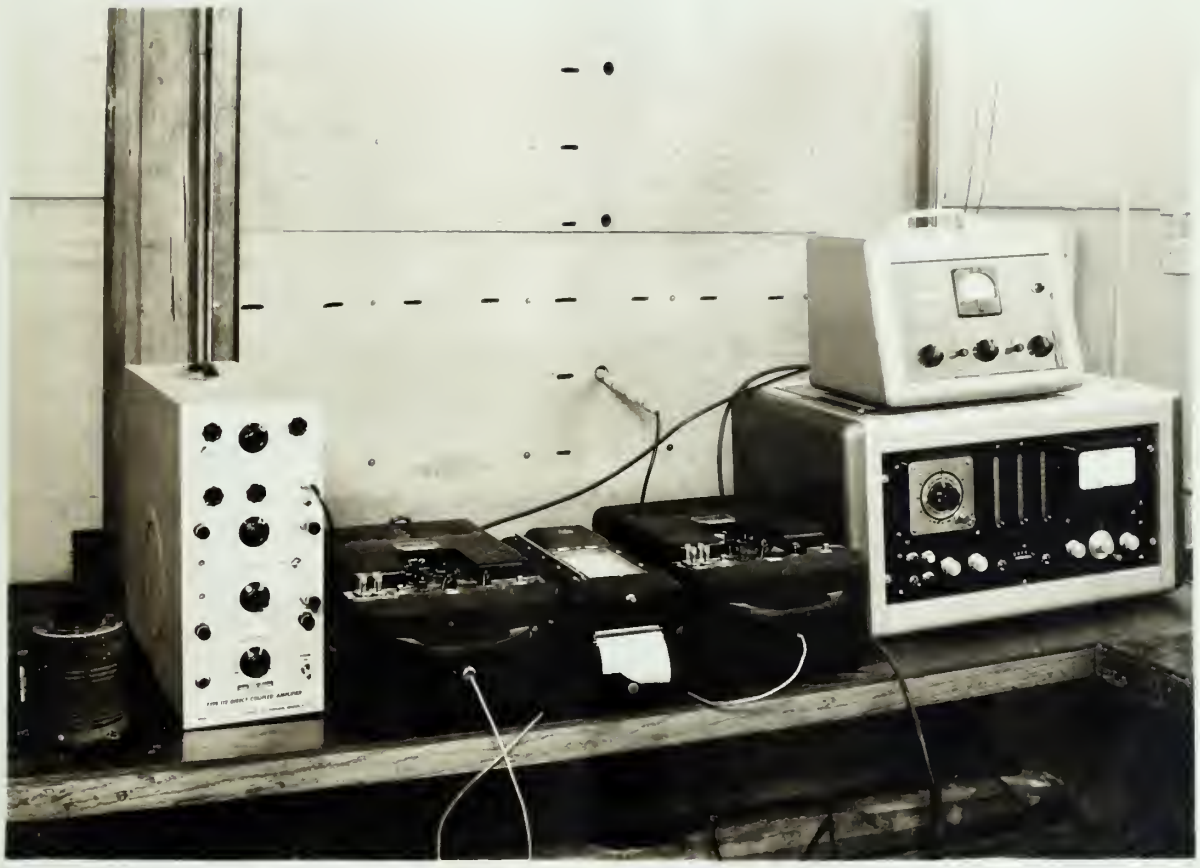

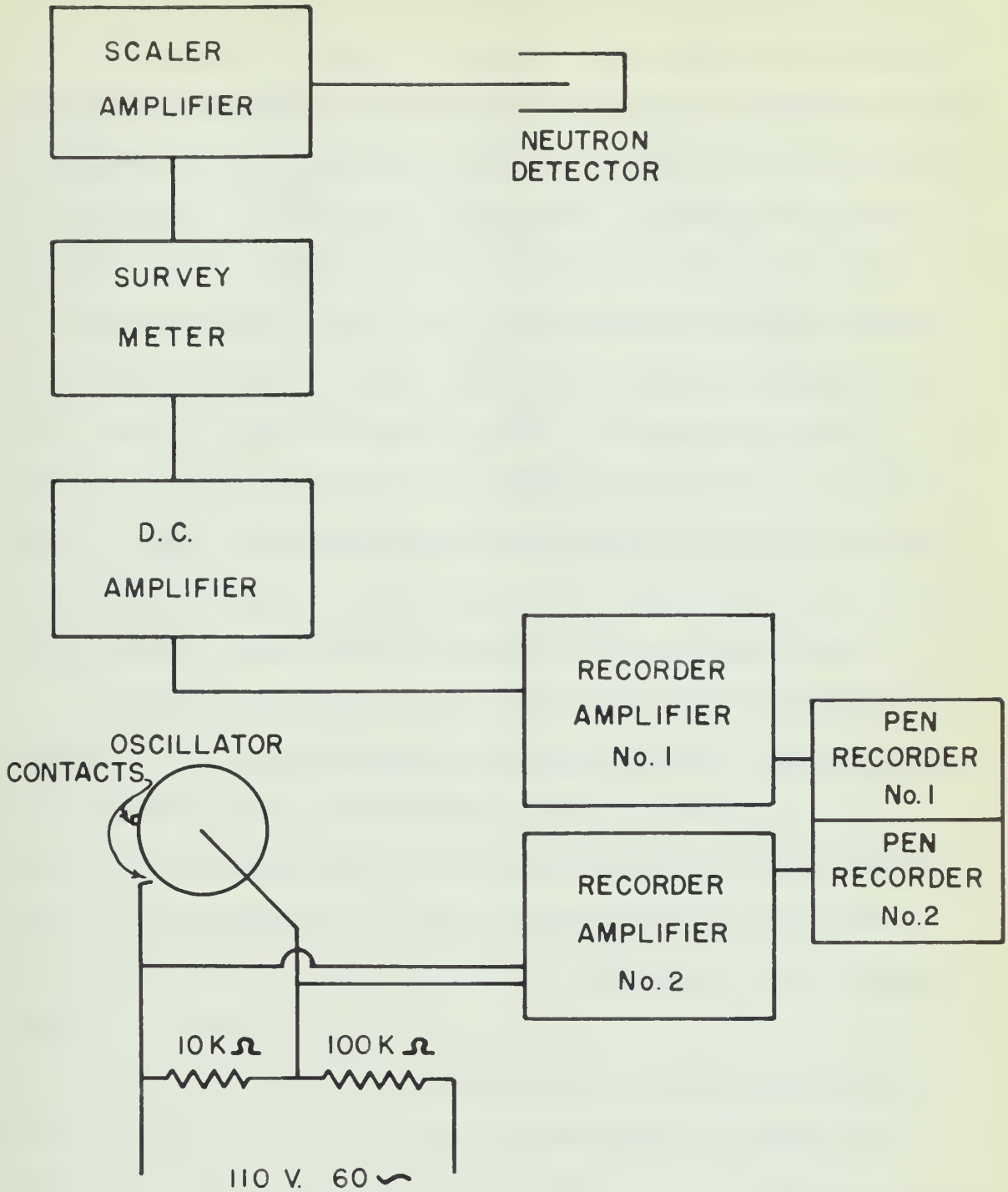

Figure 5. Electronic circuitry

to a 10K resistor as shown in Figure 5. The 10K resistor was in series with a 100K resistor, and a 110-volt 60-cycle voltage was impressed across them. The second recorder amplifier and pen were also connected across the 10K resistor. With the rotor contacts open, a 10-volt 60-cycle imput signal was plotted by the pen. Whenever the rotor contacts closed, this signal was shorted out. The brush contact mounted on the frame was approximately 120 degrees from rotor top dead center while the rotating contact was set about at point A on the rotor. It was found that oscillator speeds up to about 300 RPM could be measured in this manner. At faster speeds the length of time the wave is shorted is only a portion of one wave cycle and is very difficult to read with the rather slow pen response.

Readings were taken with the oscillator steady in positions 1 and 2 to determine the maximum range. This simulated an infinitely slow oscillation. The difference in the readings was called S_1'. Readings were then taken with the oscillator rotating at various speeds, and for each frequency the peak to peak amplitude, called n_1', was compared with the base value S_1'.

The phase angle was determined by plotting position 1 of the rotor on the time wave and comparing it with the position of peak flux for each cycle. It was noticed during preliminary tests that moving the probesteadily in and out

of the pile by hand produced a recorded wave having an amplitude less than that ultimately recorded if the probe were permitted to stop in the pile for eight to ten seconds. The pen, however, seemed to respond in phase with the motion. It was therefore decided to correct the recorded amplitude for the two second time constant of the survey meter and to accept the recorded phase angle as being approximately correct.

Because the theoretical circuit analysis appeared to be too lengthy, it was decided to obtain an amplitude correction experimentally. A sine wave signal generator was connected to the survey meter input and adjusted to give a 2-volt output. The scaler amplifier was not included in the test circuit because of the internal circuitry modifications that would have been entailed with the inclusion. Since the scaler amplifier was in essence amplifying spike voltages with a five microsecond resolution, it was considered to have negligible effect on the variation of the recorded signal amplitude. The signal generator frequency was increased until the survey meter registered 20,000 counts per minute which was approximately the same as the reading obtained with the probe inserted to the pile midpoint in the first hole. It had been noted prior that as the oscillator was rotated very slowly, the survey meter reading varied between approximately 19,000 counts per minute and 21,000 counts per minute.

The signal generator was adjusted until the survey meter read these values, and the extremes were marked on the dial. The sinusoidal variation between these extremes was obtained by attaching a yardstick solidly to the signal generator dial to permit a pendulum action. A heavy weight was clamped at various distances on the yardstick and swung to simulate the different cycling frequencies. With the pendulum held in the extreme positions the amplitude difference, as before, simulated an infinitely slow cycling speed. The ratio of the observed peak to peak amplitude at any one frequency to the amplitude difference determined above was taken as the correction factor for that frequency. The amplitude correction curve is plotted in Figure 6. The range of readings for the correction curve was severely limited by the pendulum length. Because of the physical arrangement, pendulum lengths less than 15 inches were not feasible. This was not a serious handicap since shorter pendulum lengths corresponded to faster cycling speeds which were beyond the upper values of the experimental data. The 30 inch limitation of the yardstick, caused by mounting on the dial, corresponded to a frequency of 3.59 radians per second using simple pendulum theory. It is to be noted that to obtain a frequency of one radian per second a 32.2-foot pendulum would have been needed. The correction was applied by dividing n_1' by the

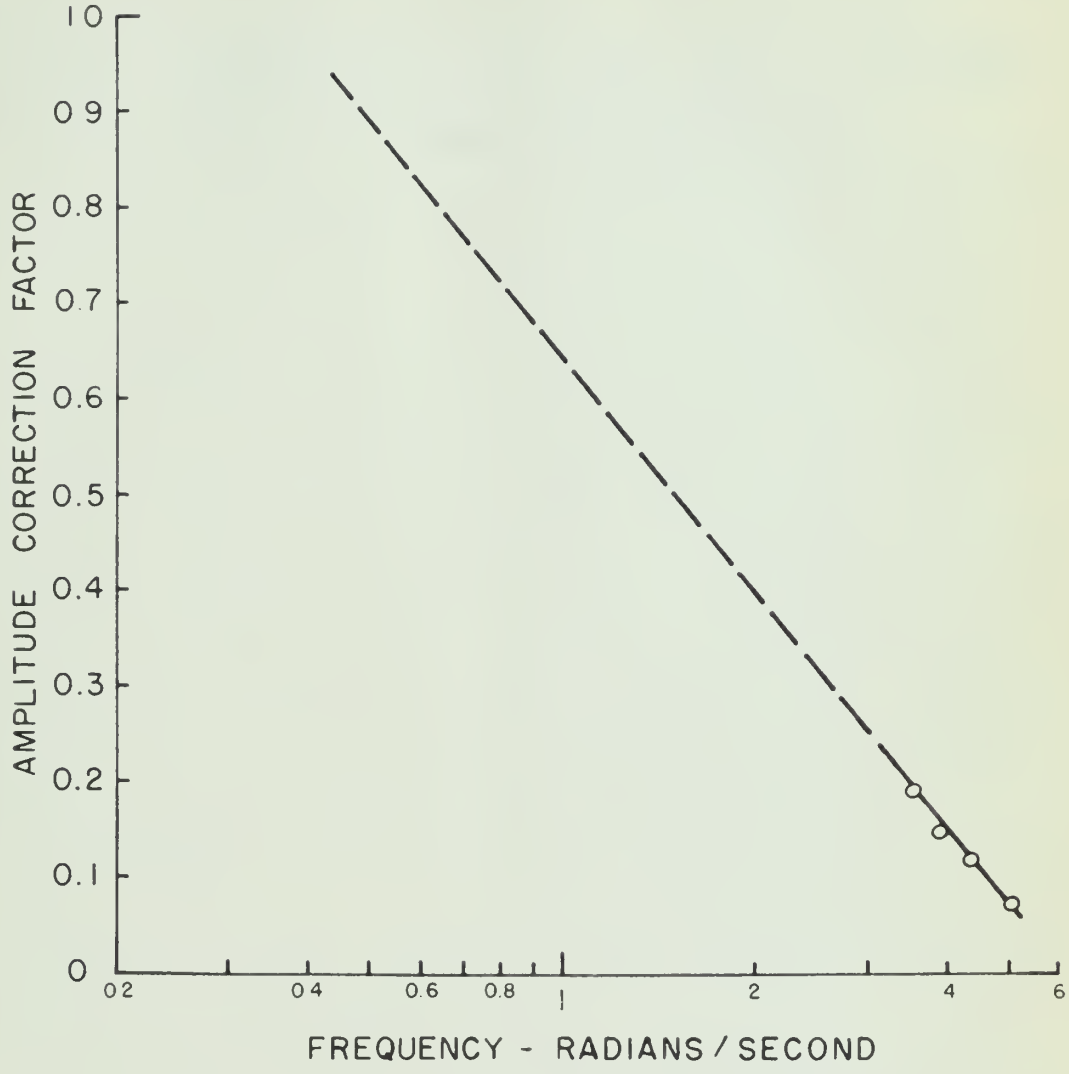

Figure 6. **Amplitude ratio correction factor vs. frequency**

corresponding correction factor at the same frequency to give the experimental values of amplitude ratio, n_1/S_1', plotted in Figure 7.

Some test runs were attempted using the second and third holes but the data were not readable. Apparently the statistical variations were of the same order of magnitude as the flux variations, masking the desired signal.

DISCUSSION OF RESULTS

The primary results of the experiment are presented graphically in Figures 7 and 8. The data from which these figures were drawn are tabulated in the Appendix.

The smooth curves are plots of Equation 28 for different values of the mean neutron lifetime in a finite assembly and for different values of k. Since neither ℓ nor k have been determined for the assembly in question, values of k = 0.7 and 0.8 and ℓ = 0.07 seconds and 0.1 seconds were chosen to indicate the trend of the curves with both ℓ and k and to indicate the general curve shape. In the theoretical derivation the six groups of delayed neutrons were replaced with an average group to reduce the amount of computation. With the total fraction β of the delayed neutrons equal to 0.0073, an average λ equal to 0.08 seconds^{-1} was computed from $\lambda = \frac{\sum_{i=1}^{6} \beta_i \lambda_i}{\beta}$ (6, p. 230). With the above parameters in the Equation 28, the amplitude ratio and phase angle were determined for various frequencies.

Measurements of the neutron flux in the first hole were taken for oscillator speeds from approximately 0.5 to 5 radians per second. Both phase angle and amplitude ratio readings were obtained. The recorded phase angle is plotted

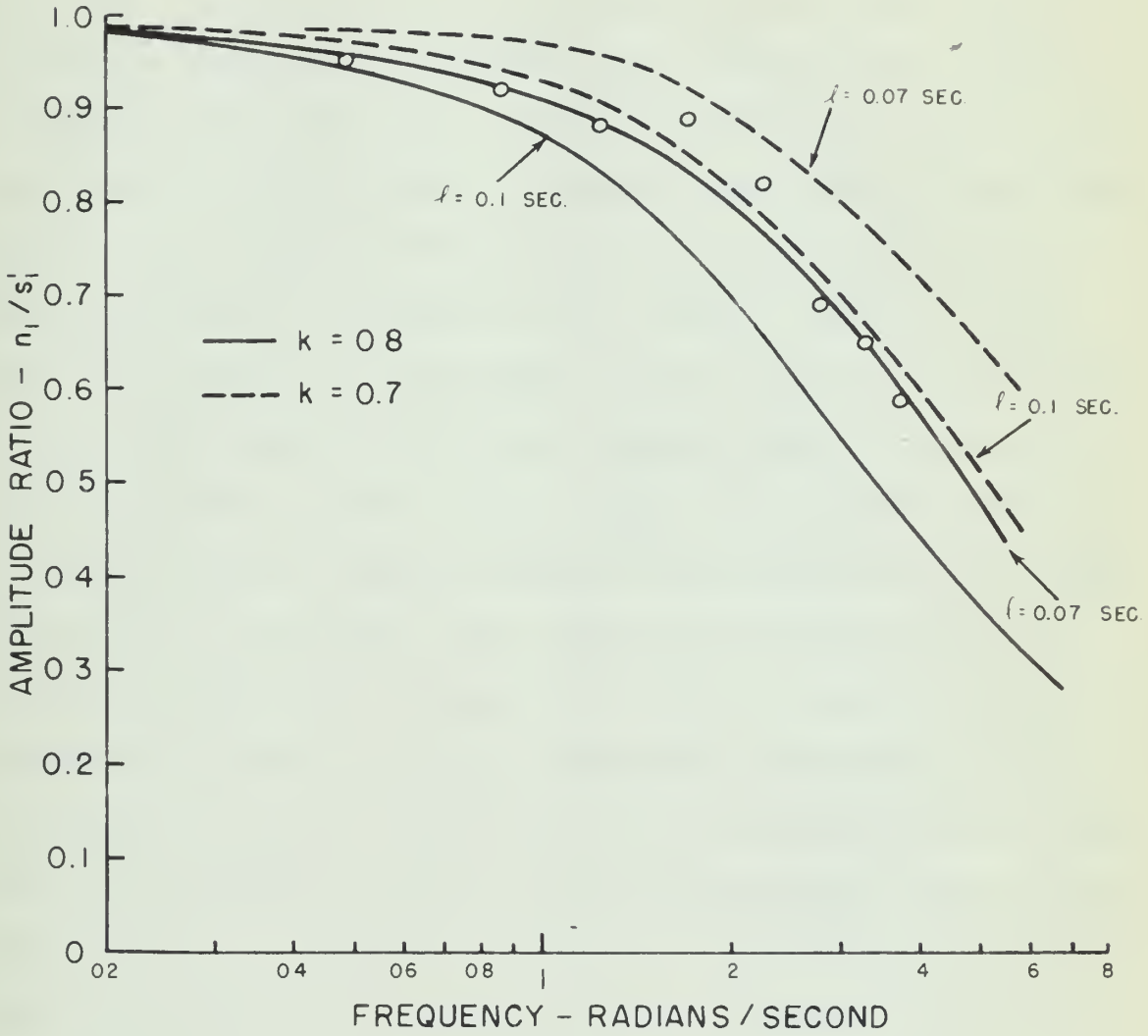

Figure 7. Amplitude ratio vs. frequency

in Figure 8. The recorded amplitude ratios were corrected for the two second time constant of the survey meter by the correction factor indicated in Figure 6. The data for the amplitude ratio correction factor, tabulated in the Appendix, plots as a straight line on semi-logarithmic paper. The range was increased by straight line extrapolation. This result is valid only over a limited range since for all frequencies the factor cannot be greater than unity or less than zero. Hence the true factor must deviate somewhat from a straight line as it approaches the extreme values. At the lower frequencies the correction factor itself becomes small, so the above deviation will have little effect on the corrected amplitude ratio. At the higher frequencies where the correction factor becomes large in comparison to the readings the effect is magnified, and extreme care would need to be taken to justify any extrapolated values. Fortunately the frequencies obtained in the experimental correction factor tests were as high as those used in the amplitude ratio tests and no extrapolated values in the high frequency range had to be used. The ω plotted in Figure 6 is actually that of the pendulum, but it corresponds directly to that of the oscillator since in both cases it is the frequency of the driving function. The frequency was solved for a simple pendulum (without damping) from the formula $\omega = \sqrt{g/\ell}$ where g is the gravitational acceleration in feet per second^2

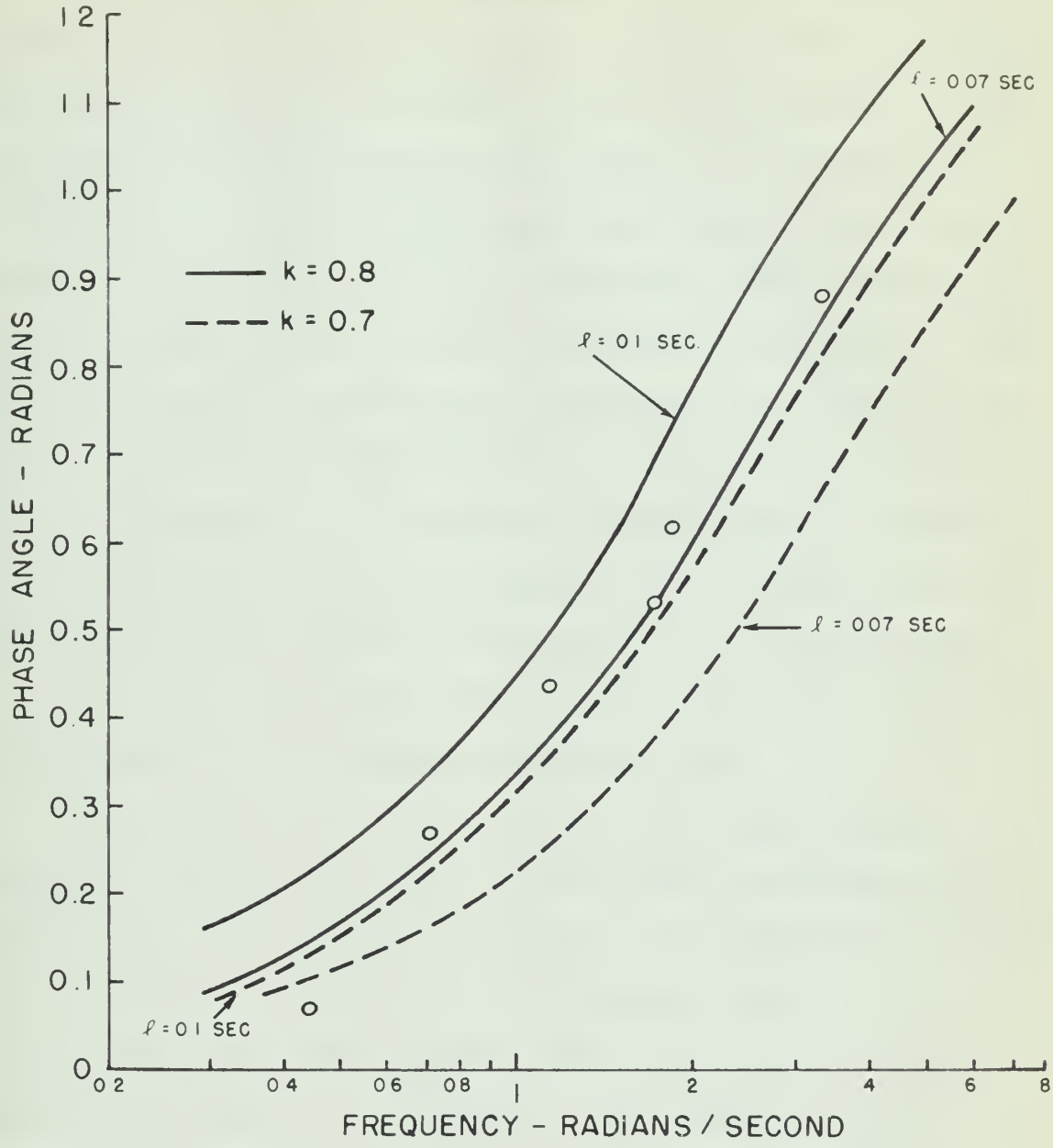

Figure 8. Phase angle vs. frequency

and ℓ is the pendulum length in feet.

An interesting result of the experiment was the decrease in median flux level with increasing ω. The value of the median line of the sinusoidal flux variation for each testing frequency was plotted in Figure 9 as it appeared on the pen recorder, with the recorder paper scale as the arbitrary ordinate scale. This value corresponds to n_0 in the theoretical development, and it is tabulated in the Appendix for each frequency tested. In the splitting of Equation 21 into the steady and the sinusoidal conditions, it is seen that n_0 has no theoretical relation with ω. Hence the observation was not predicted by the theory. The only logical explanation lies in the oscillator design and the method chosen to accomplish source forcing. No tests were run to determine the exact cause since the actual median flux level would have little effect on the cycling amplitude ratio.

Experimental uncertainty results from many factors. A very slow rotation trial run was made with the neutron probe within three inches of the oscillator to check the variation in the source. The very small distortions noted in the plotted sine wave could possibly have been due to neutron scattering, voids in the paraffin, and amplifier drift. Perhaps the greatest source of error in the experiment was the signal fluctuations due to statistical variations and noise. These variations obscured and distorted the peaks of

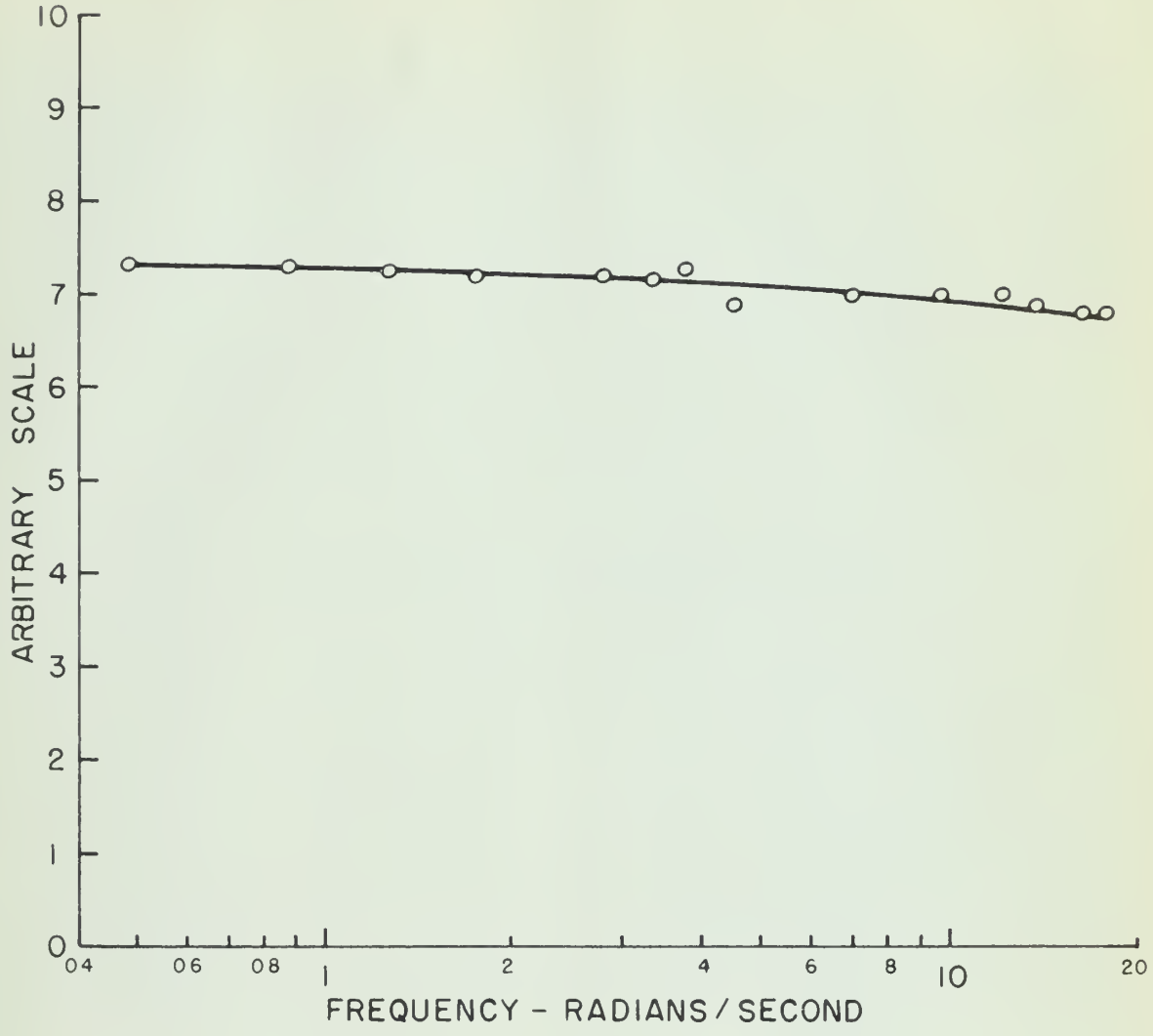

Figure 9. Median flux level vs. frequency

Figure 10. Views of typical data

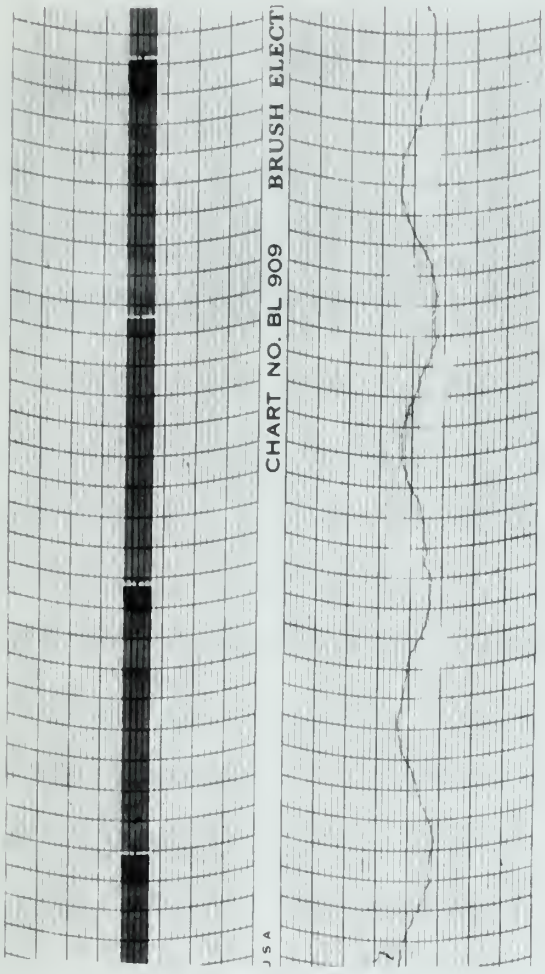

A. Low gain

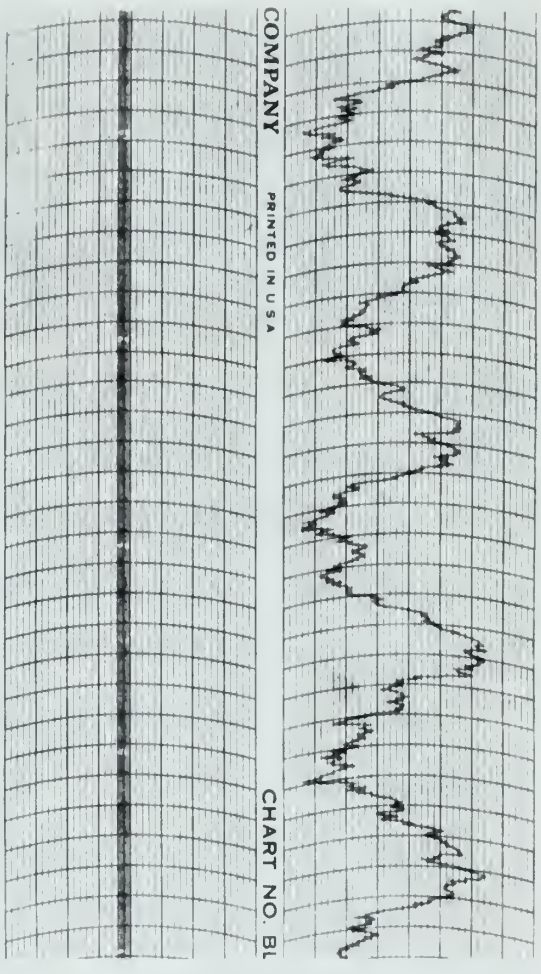

B. High gain

the signals, adding to the difficulty of determining both the amplitude ratio and the phase angle. Two samples of typical data, demonstrating readings obtained with both high and low gain, are shown in Figure 10.

To compare the experimental and calculated values of amplitude ratio and phase angle, it is only necessary to observe the shapes of the curves. It is seen that the experimental points lie reasonably close to the theoretical curve plotted for values of $k = 0.8$ and $\ell = 0.07$ seconds.

CONCLUSIONS

The transfer function determined experimentally agrees quite well with that predicted by the theory. While it was not the purpose of the thesis, the experimental points indicate a mean neutron lifetime in the assembly of approximately 0.07 seconds and an effective multiplication factor of approximately 0.8.

The rotor assembly thermalized and absorbed a sufficient percentage of neutrons to permit obtaining acceptable data from the first hole. In the second and higher holes the sinusoidal variation in the neutron flux was reduced to the order of magnitude of the statistical and noise variations and could not be read. With a larger or more efficient neutron detector, a thicker paraffin jacket, or possibly a thicker cadmium pattern, the amplitude of the sinusoidal variations could be substantially increased permitting correspondingly smaller deviations and statistical errors.

The median level of the pile neutron flux decreased with increasing cycling speed. This result is not predicted by the theory and is probably due to the design of the oscillator.

Although the experimental results were not extremely

accurate it is felt that the data can be reproduced with sufficient accuracy and consistency to substantiate the theoretical predictions.

SUGGESTIONS FOR FURTHER STUDY

It is very apparent that the possibilities in cycling a subcritical assembly have not been fully exploited. It remains to improve on and enlarge the range of readings to much faster and much slower cycling speeds. This will require some modification in the oscillator drive mechanism. Readings with a higher degree of certainty at the greater speeds can be obtained by redesigning the basic circuitry to have a lower time constant and perhaps to include a discriminator to reduce the statistical variation. Once this has been accomplished it would be desirable to obtain the transfer function of the same pile by the technique of reactivity forcing and to compare the results of the two methods.

All the suggestions above pertain to the assembly itself as being the object of investigation. With the background knowledge of the transfer function, the whole area of investigating the utilization of the subcritical assembly as a facility for testing components and for advanced design research will have been opened.

LITERATURE CITED

1. Allardice, Corbin, and Trapnell, Edward R. The first pile. Atomic Energy Commission [Document] TID-292 [Technical Information Division]. Oak Ridge, Tenn., U. S. Atomic Energy Commission. Dec. 13, 1949.

2. Axtmann, R. C., Dessauer, G., and Parkinson, T. F. Reactivity measurements in a subcritical pile. Atomic Energy Commission [Document] DP-48 [E. I. du Pont de Nemours and Co.] . Augusta, Ga., Savannah River Laboratory. November 1955.

3. Boland, J. F., Smith, L. N., and Nice, R. E. A measurement of the transfer function of a fast critical assembly. Argonne National Laboratory [Document] ANL-5782. Washington, D. C., Office of Technical Services. September 1957.

4. Brown, Gordon S., and Campbell, Donald P. Principles of servomechanisms. New York, N. Y., John Wiley and Sons, Inc. 1948.

5. Franz, Joseph P. Pile transfer functions. Atomic Energy Commission Declassified [Document] AECD-3260. Oak Ridge, Tenn., Technical Information Service. July 18, 1949.

6. Glasstone, Samuel. Principles of nuclear reactor engineering. Princeton, N. J., D. Van Nostrand Co., Inc. 1955.

7. _____ and Edlund, Milton C. The elements of nuclear reactor theory. Princeton, N. J., D. Van Nostrand Co., Inc. 1952.

8. Harrer, J. M., Boyar, R. C., and Krucoff, D. Transfer function of Argonne CP-2 reactor. Nucleonics 10, no. 8: 32. 1952.

9. Owens, J. I., Jr., Crever, F. E., and Pigott, J. H. A proposed automatic control system for the Schenectady reactor. Atomic Energy Commission Declassified [Document] AECD-4209. Oak Ridge, Tenn., Technical Information Extension. March 29, 1949.

10. Pigott, J. H., and Owens, J. I. Control of an atomic power plant. Atomic Energy Commission Unclassified [Document] AECU-1511. Oak Ridge, Tenn., Technical Information Service. May 11, 1951.

11. Schultz, M. A. Control of nuclear reactors and power plants. New York, N. Y., McGraw Hill Book Co., Inc. 1955.

ACKNOWLEDGMENTS

The author wishes to thank Dr. Robert E. Uhrig for the original suggestion of this project and for his interest and patient assistance. Many thanks are due Dr. Glenn Murphy, Head of the Department of Theoretical and Applied Mechanics and Chairman of the Nuclear Engineering Administrative Committee, for his assistance in securing the instrumentation required for completion of this work. As is true in any project undertaken, the associations and occasional meetings are too numerous for an individual recountal, but an acknowledgment would not be complete without expressing sincere gratitude to the many persons who have given suggestions and encouragement throughout the entire course of the work.

The author would also like to express his appreciation to the U. S. Naval Postgraduate School for the educational opportunities afforded and to the United States Navy for making all this work possible.

APPENDIX

Table 1. Amplitude ratio correction factors

l inches	l feet	ω^2 (= g/l)	ω radians/second	Correction amplitude	Correction factor
30	2.5	12.57	3.59	0.95	0.19
25	2.08	15.5	3.94	0.75	0.15
20	1.66	19.35	4.4	0.6	0.12
15	1.25	25.7	5.08	0.35	0.07

Table 2. Amplitude ratio data

Run	ω radians/second	n_1'	$\frac{n_1'}{S_1'}$	$\frac{n_1}{S_1'}$
12	0.49	0.85	0.85	0.95
13	0.87	0.65	0.65	0.92
14	1.26	0.5	0.5	0.88
15	1.73	0.4	0.4	0.89
16	2.25	0.3	0.3	0.82
17	2.78	0.2	0.2	0.69
18	3.31	0.15	0.15	0.65
19	3.73	0.1	0.1	0.59

Table 3. Phase angle data

Run	ω radians/second	Phase angle-radians
1	0.44	0.07
2	0.715	0.27
3	1.15	0.44
4	1.73	0.53
5	1.85	0.62
6	3.31	0.88

Table 4. Median flux levels

ω radians/second	Level
0.49	7.3
0.87	7.3
1.26	7.25
1.73	7.2
2.78	7.2
3.31	7.15
3.73	7.3
4.54	6.9
6.98	7.0
9.67	7.0
12.2	7.0
13.9	6.9
16.4	6.8
17.9	6.8

thesR374
Transfer function of a uranium-graphite
3 2768 001 91272 8
DUDLEY KNOX LIBRARY